Supplementary Information

A simple microfluidic device for live-imaging of the vertical section of epithelial cells

Seigo Araki,[a†] Masayoshi Nakano,[a†] Mamiko Tsugane,[b,c] Fumiko Sunaga,[b] Mitsuru Hattori,[d,e] Masahiro Nakano,[d] Takeharu Nagai[d,e] and Hiroaki Suzuki[*a, b]

[a.] Precision Engineering Course, Graduate school of Science and Engineering, Chuo University, 1-13-27 Kasuga, Bunkyo-Ku, Tokyo, 112-8551, JAPAN.
*E-mail: suzuki@mech.chuo-u.ac.jp
[b.] Dept. Precision Mechanics, Faculty of Science and Engineering, Chuo University, 1-13-27 Kasuga, Bunkyo-ku, Tokyo, 112-8551, JAPAN.
[c.] Japan Society for the Promotion of Science (JSPS), 5-3-1 Kojimachi, Chiyoda-ku, Tokyo, JAPAN.
[d.] Graduate School of Frontier Biosciences, Osaka University, 1-3 Yamadagaoka, Suita, Osaka, 565-0871, JAPAN.
[e.] The Institute of Scientific and Industrial Research, Osaka University, 8-1 Mihogaoka, Ibaraki, Osaka 567-0047, JAPAN.
[†] These authors contributed equally to this work.

Supplementary Text: Evaluation and Determination of Index of Resolution (IoR)

In this work we opt to quantitatively compare the relative resolution of fluorescent microscope images of microtubules as a model organelle. For this purpose, we employed Sobel filtering operation, a major image filter for detecting edges of objects (the actual operator is explained in the main text). A seen in Fig. S1, edges of the filaments with high contrast produce high-intensity values after filtering (Fig. S1a), whereas those in a blurred image produce smaller values (Fig. S1b). We employed the average of the intensity distribution of the filtered images as the Index of Resolution (IoR).

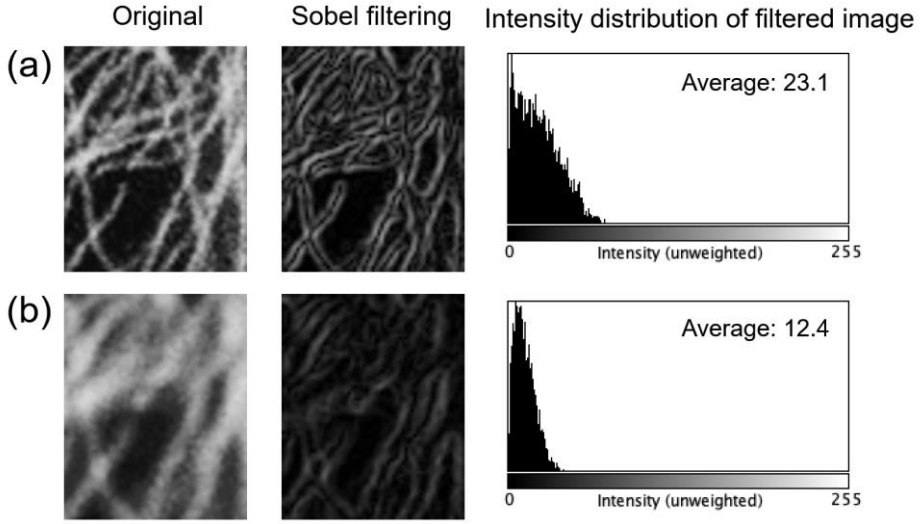

Fig. S1 Comparison of the results of Sobel filtering operation performed for (a) a high-contrast image and (b) the low contrast image. The intensity values in the filtered image for (a) are high at the edge portion of filaments. Average intensity values of all pixels in the image were employed as IoR. (Note that the intensity of filtered images (middle) is doubled only for improving visibility).

However, this definition of resolution cannot be applied universally. First, this index value depends on the brightness of the image, which is affected by the expression level of GFP-tagged tubulin. Second, it also depends on the number of microtubules in images. To remedy the variability of these parameters, we randomly selected ten cells in the same device and used the small section of each image of tubules that overlap with the nucleus. In this part of the cell, microtubules extend nearly in the 2D plane under the nucleus. The section of the image sample is 9.9 μm × 9.9 μm (50 × 50 pix; ~0.2 μm/pix). Since the persistence length of microtubules is more than a millimeter, filaments should appear nearly straight in this window.

In the following part, we evaluate the adequacy of our definition of IoR. First, we checked if the IoR values reflect the in-focus and out-of-focus images of microtubules. For this purpose, we obtained the stuck of sliced images of a cell with 1 μm z-spacing (Fig. S2a-1; Raw images) and evaluated IoR. As plotted with the orange line in Fig. 2(b), the result showed a bell-shaped curve with a peak value at the in-focus image. However, we noticed that the out-of-focus images are darker. This fact implies that, even if the sharpness of images is the same, the darker image could result in smaller IoR value because Sobel filtering takes the spatial gradient of the intensity.

Thus we tested if the intensity adjustment improves this ambiguous situation to compensate for the brightness/darkness of the image. Although there are many schemes to modulate the intensity distribution of images, we employed the most straightforward method; the Mathematica function "ImageAdjust," which rescales the intensity distribution of the 8-bit image to cover the range zero to 255 (Fig. S2a-2). The result is plotted as the gray line in Fig. S2(b). It also showed the bell-shape curve around the focal plane, but the IoR value also increased in planes away from the focus. This fictitious result comes from the random noise enhanced by rescaling. To further remedy this effect, we applied the median filter to rescaled images, which is known to suppress the random noise (Fig. S2a-3). As plotted with the blue line in Fig. S2(b), the fictitious high value is reduced, whereas the width of the fibers in the image is not broadened.

Next, we tested the compensation of the number of microtubules in the image. If the brightness and sharpness of microtubules are the same, both the sum of the intensity of the original image and the resultant IoR value should be merely proportional to the number (more precisely, total length) of fibers. Thus, we re-plotted Fig. S2(b) by normalizing IoR with the average intensity value (0–255 scale) of each original image. The result (Fig. S2c) shows the same bell-shape distribution but with similar magnitudes among three lines, because this operation normalizes the gradient values of individual filaments.

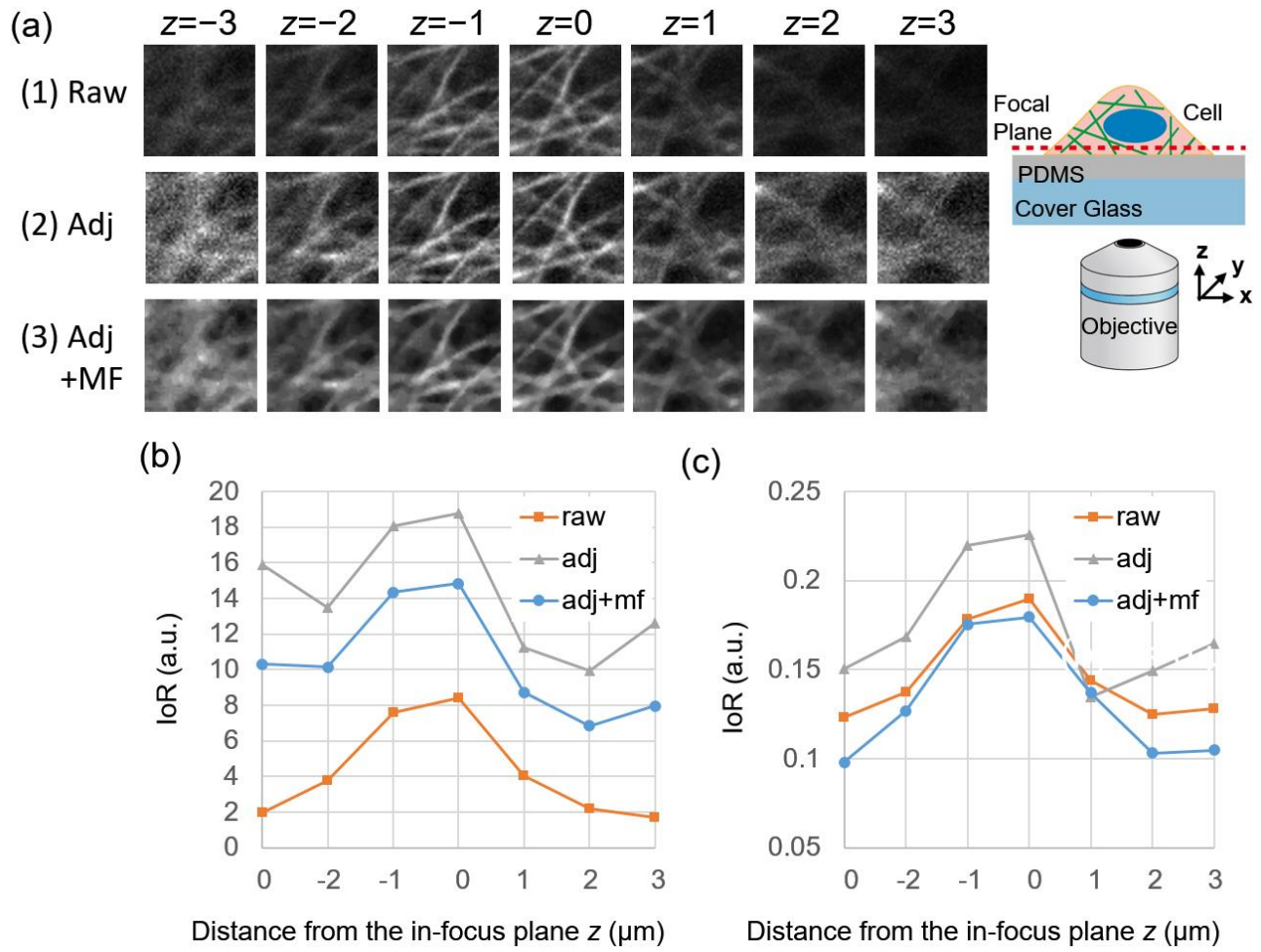

Fig. S2 (a) Images of microtubules obtained with 1 μm z-spacing. (1) Raw images. (2) Images after the intensity adjustment. (3) Images after intensity adjustment followed by the median filtering. (b, c) Results of IoR evaluation. (b) IoR values obtained by applying the Sobel filter directly to images shown in (a). (c) IoR values normalized by the averaged intensity of each image.

Next, we tested if our definition of IoR properly represents the contrast of the microtubule images. We applied the six procedures discussed in Figs S2(b) and (c) to microtubule images obtained for the evaluation of different PDMS thicknesses (Fig. 2 in the main text). All images processed are displayed in Fig. S5, in which 10 to 20 microtubule filaments are visible in most of the cases. The direct evaluation of IoR to raw images (Fig. S3a) shows the nice monotonically decaying curve against the PDMS thickness. However, the raw images obtained for the thicker PDMS layer appear darker with the identical microscope setting. When these IoR values are normalized by the averaged intensities, we still achieved the monotonically decaying curve (Fig. S3b), but variability among each PDMS thickness became larger. Next, we evaluated IoR to images with intensity adjustment. In this case, the profiles became nearly flat against the PDMS thickness (both with and without intensity normalization; Figs S3c and d). This result came from the noise enhanced by the intensity recalling to very dark images, as already discussed in Fig. S2(b) and (c). Lastly, we evaluated IoR to images, to which intensity adjustment followed by the median filtering is applied. Although this procedure without intensity normalization results in the relatively flat profile (Fig. S3e), that with

intensity normalization showed a monotonically decaying curve with smaller deviations (Fig. S3f). This difference comes from the fact that, in originally very dark images with undistinguishable fibers, the overall brightness levels after intensity adjustment became large. Hence, the intensity normalization suppressed this artifact.

In the manuscript, we employed the result with normalized IoR after intensity adjustment and median filtering (Fig. S3f), which takes the variability of brightness level (i.e., the expression level of GFP) and amount of microtubules into account.

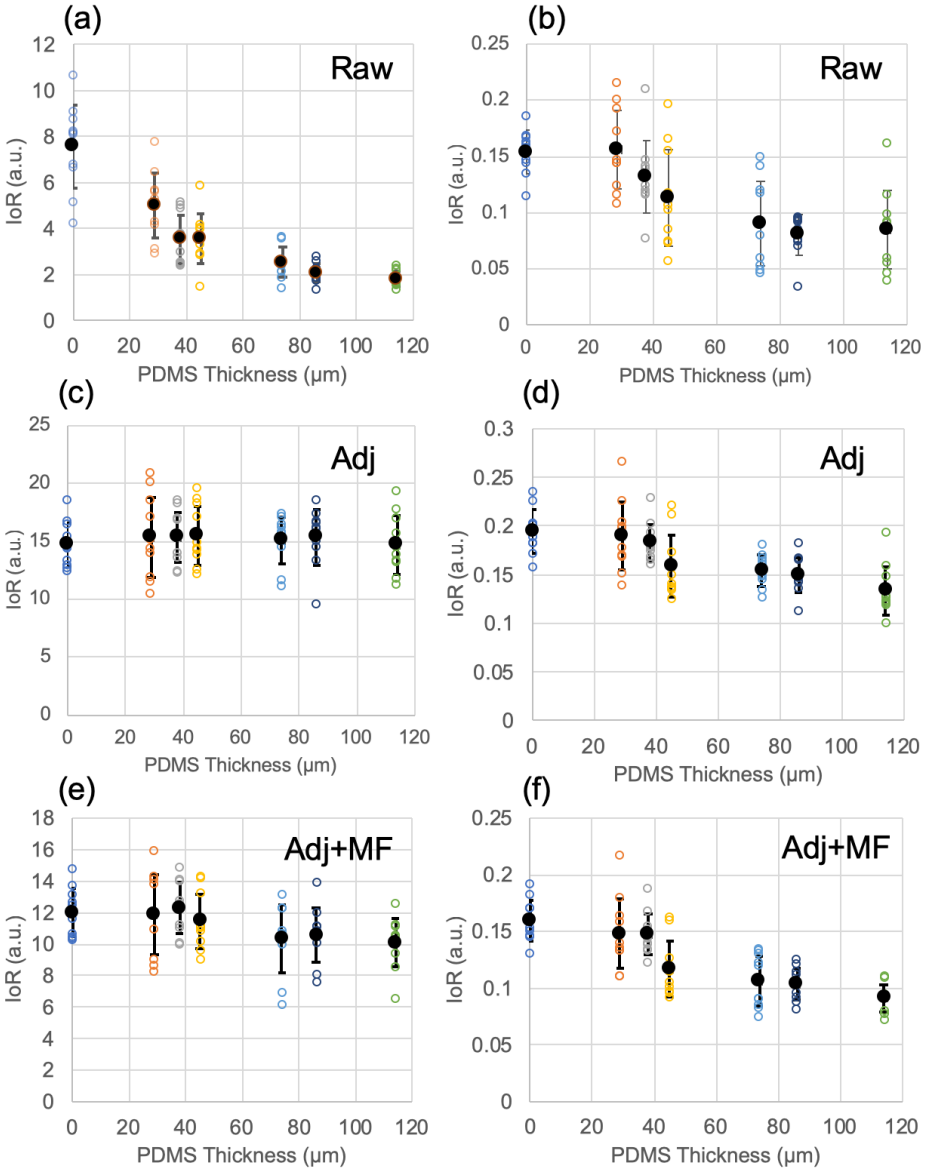

Fig. S3 Results of the evaluation of IoR for microtubule images obtained on the PDMS layer having various thicknesses. In all figures, open circles represent all IoR values for individual images, while solid black circles and corresponding error bars represent the average values and standard errors for each condition. (a) IoR for raw images. (b) IoR normalized by the average intensity for raw images. (c) IoR for images with intensity adjustment. (d) IoR normalized by the average intensity for images with intensity adjustment. (e) IoR for images with intensity adjustment and median filtering. (f) IoR normalized by the average intensity for images with intensity adjustment and median filtering.

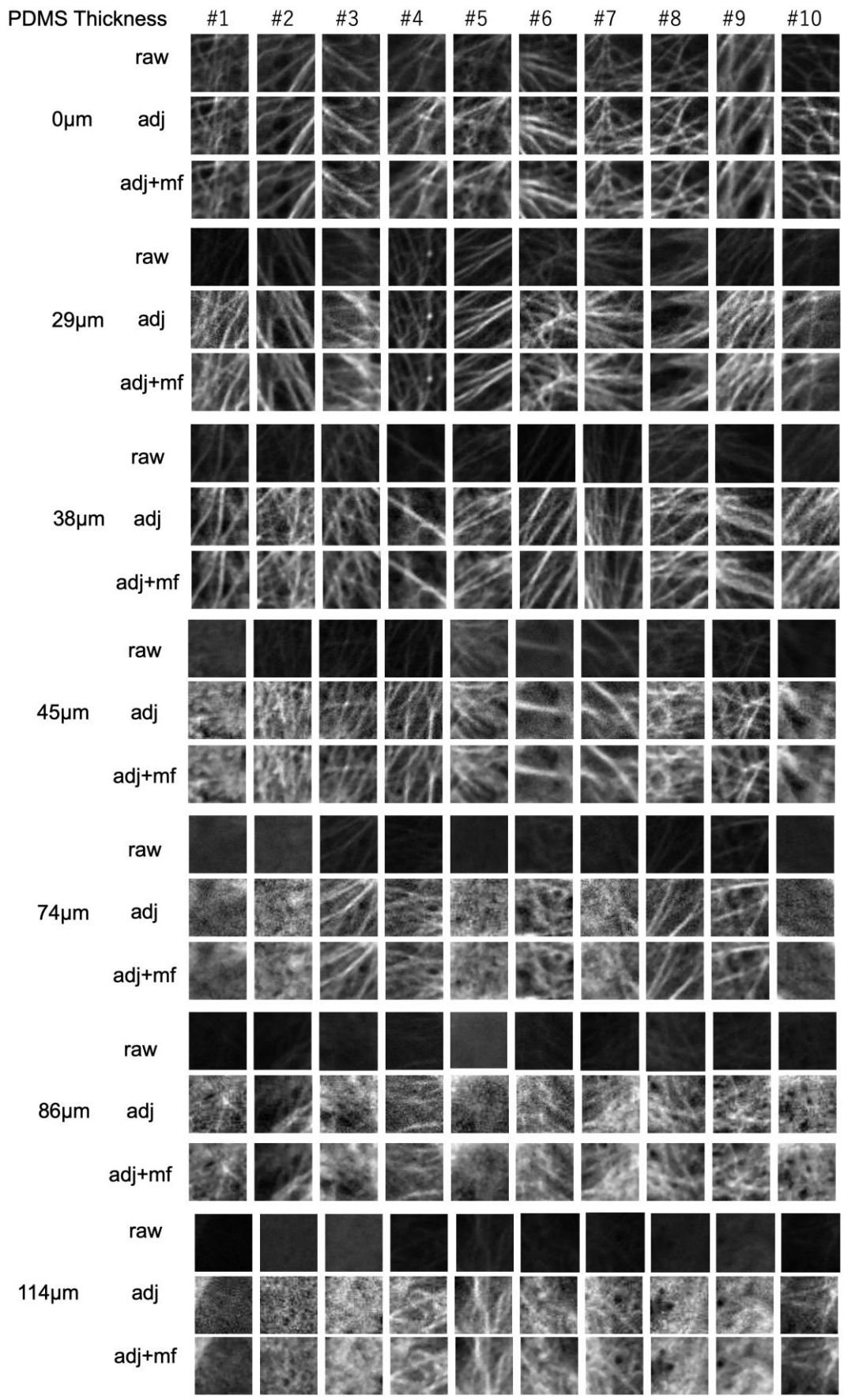

Fig. S4 All image data used to evaluate Fig. S2 in the main text and Fig. S3 in the supplementary information.

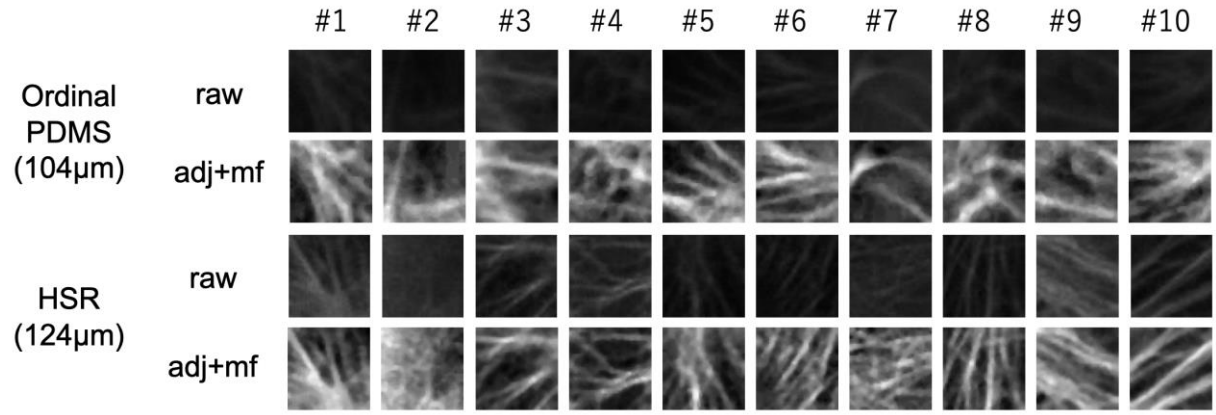

Fig. S5 All image data used to evaluate Fig. 3 in the main text.

(a)

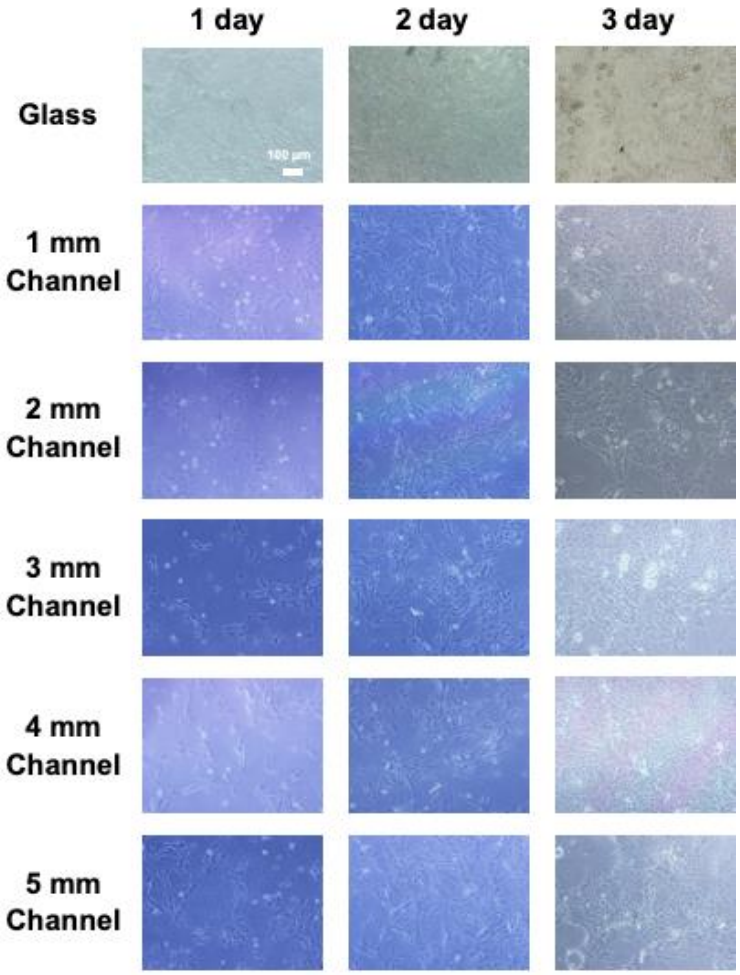

(b)

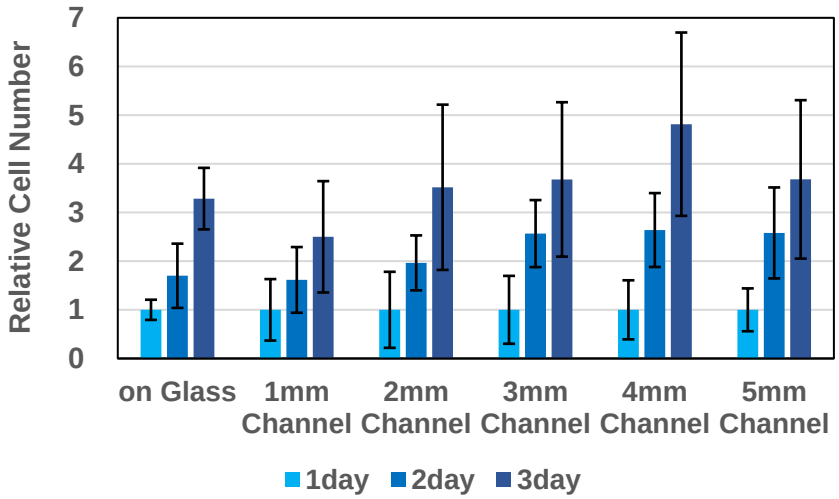

Fig. S6 (a) Growth of MDCD cells cultured in the closed channel device (CCD) having various widths. (b) Cell density relative to the culture on a regular culture on a glass device (1st day).

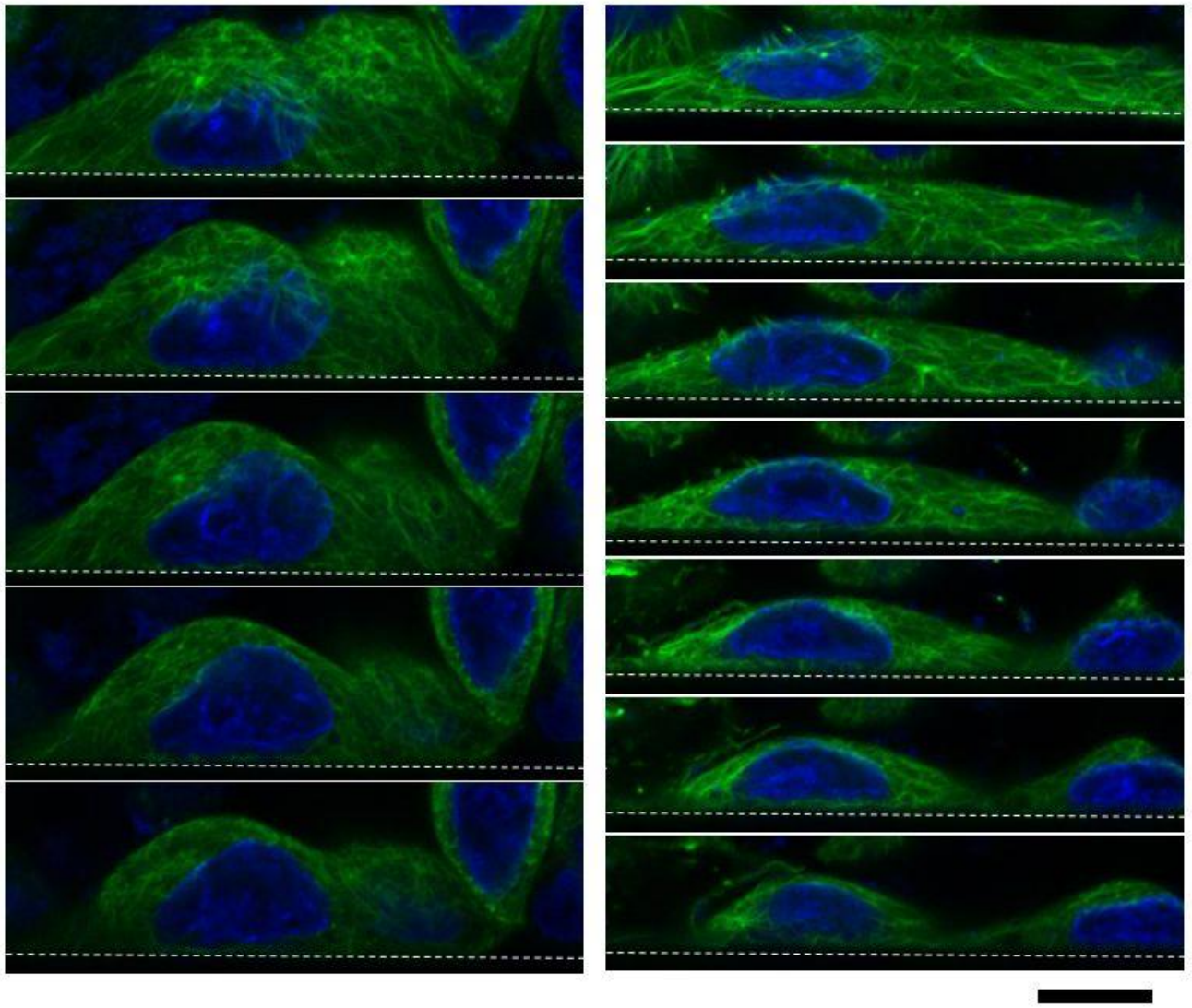

Fig. S7 Two examples of *z* stuck of vertical images obtained with CCD. The *z* interval of each image is 1 μm (positive increment of z in the coordinate shown in Fig. 4c-e), and the scale bar indicates 10 μm. White dotted lines indicate the sidewall of the channel. Microtubule fibers (green) can be seen in all images. Blue color represents nucleus.

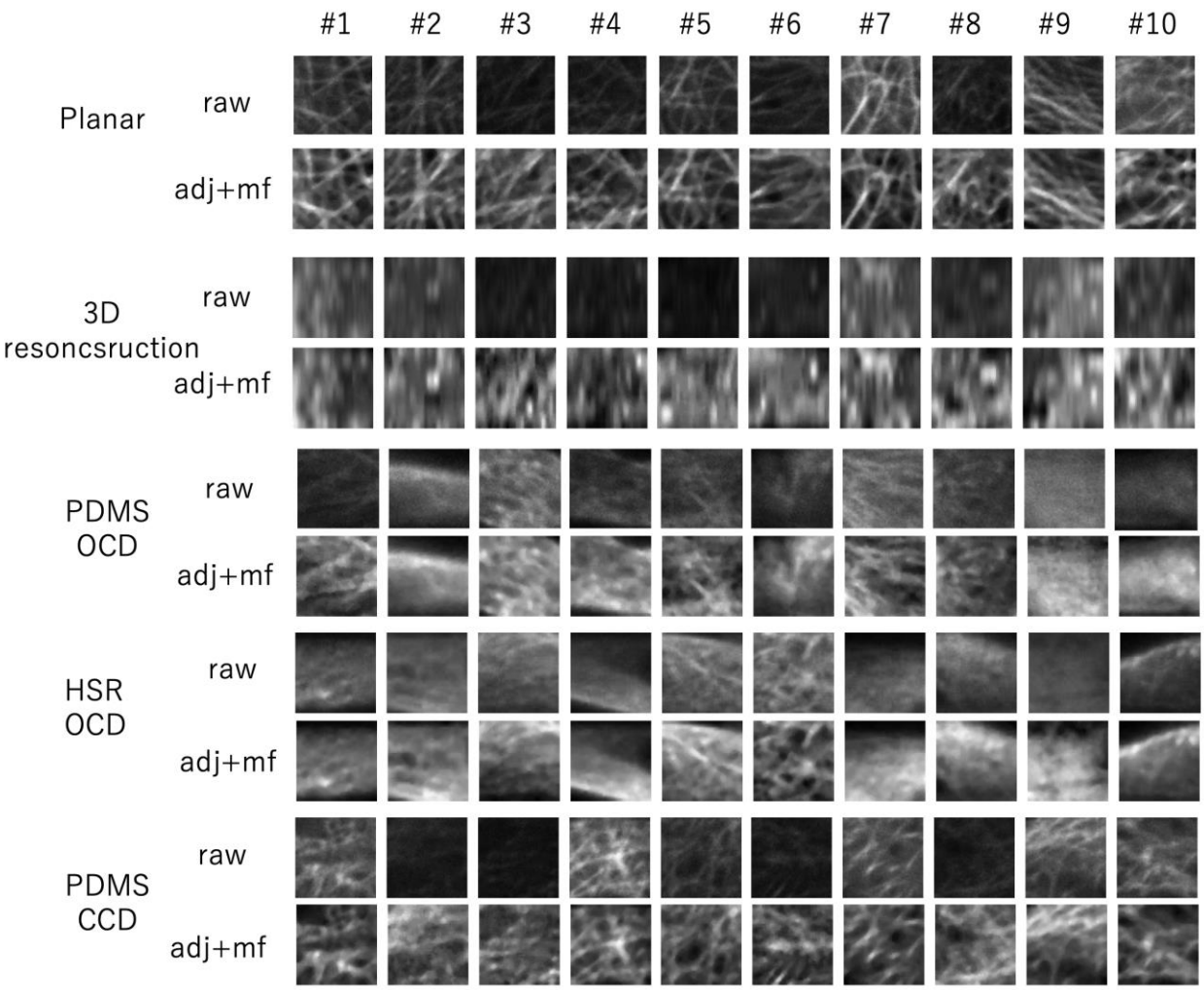

Fig. S8 All images used to evaluate Fig. 4 in the manuscript. Images obtained by the 3D reconstruction of many sliced images (the second set) are shown only for reference. In these images, microtubule filaments are not visible, but they produce fictitious values of IoR due to the mere fluctuation of the intensity.

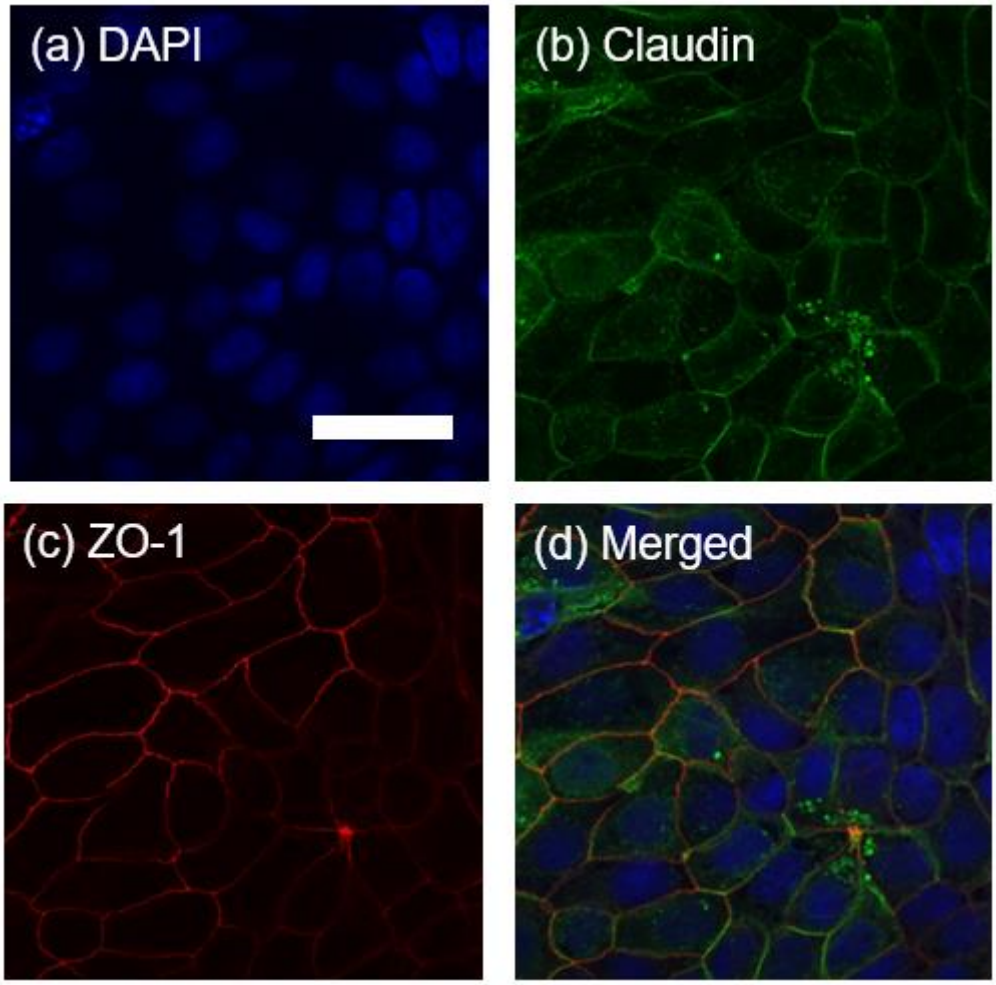

Fig. S9 Planar imaging of …Ordinal planar imaging of fixed MDCK cells. Blue: Hoechst 33342, Green: Claudin 4-GFP, Red: Immuno-stained ZO-1.

Movie S1 Live sectional imaging of mitochondria of MDCK cells obtained at 1s interval. Top: fluorescence images, bottom: bright-field images.